Sensors & Actuators: B. Chemical 368 (2022) 132231

Contents lists available at ScienceDirect

Sensors and Actuators: B. Chemical

journal homepage: www.elsevier.com/locate/snb

Two-dimensional manipulation of droplets on a single-sided continuous optoelectrowetting digital microfluidic chip

Enqing Liu, Cui Wang, Hanyun Zheng, Shuren Song, Antoine Riaud *, Jia Zhou *

State Key Laboratory of ASIC and System, School of Microelectronics, Fudan University, Shanghai, PR China

ARTICLE INFO

Keywords:
Optoelectrowetting
Z-shaped pattern control
Two-dimensional manipulation

ABSTRACT

Digital microfluidic chips are liquid processors that perform biochemical assays by moving, merging and splitting droplets using the electrowetting effect. Yet, hardwiring electrowetting chips becomes tedious as soon as they include more than a few dozen electrodes. Single-sided continuous opto-electrowetting, where the electrowetting effect of a featureless semiconductor film is controlled by light patterns is a promising solution to this hardwiring bottleneck, but so far two-dimensional manipulation of droplets is still difficult. Here, we demonstrate the manipulation of droplets along arbitrary directions by using Z-shaped light patterns that rotate the electric field by an arbitrary angle. We provide a theoretical model for driving droplets in different directions. It is verified by Comsol simulations and experiments. Optimization of the width of the notches provides quite large increase of the driving voltage in the y-direction. The chip can move dyed water droplets in the y-direction at a maximum speed of 4.86 mm/s. Such multidimensional droplet driving opens new possibilities for single-sided continuous optoelectrowetting such as merging droplets that are not in line, efficient droplet mixing, and bypassing droplets to avoid coalescence.

1. Introduction

Lab-on-a-chip technology is revolutionizing analytical biochemistry [1,2], cell biology [3,4] and sample trace detection [5,6], due to its advantages of high throughput and small size. Digital microfluidics, such as electrowetting on dielectric (EWOD), allows programming of microfluidic chips [7,8] and shows significant potential in digital PCR [9,10], digital ELISA [11,12] and other techniques.

EWOD technology uses pixelated electrodes to perform series of operations such as droplet generation, transportation and mixing. As the volume of droplets manipulated by EWOD decreases and the number increases, the EWOD chip layout faces scaling-down challenges such as a wiring bottleneck, limited number of pins, complex control signals, crosstalk, etc [13,14]. Furthermore, the volume, position and number of droplets are restricted by the fixed size and location of the electrodes [15,16]. In 2003, Chiou et al. invented the opto-electrowetting (OEW) technology that addresses this wiring issue [17,18] by using photoconductive materials as light-activated electrodes. These sandwiched OEW devices [19–21] can realize all elementary droplet operations in two dimensions. However, the presence of the top electrode not only complicates integration of OEW actuation with other functions such as droplet identification and detection, but also requires additional lithography steps and results in microrough surface prone to droplet pinning. The same group then proposed a simpler single-sided continuous optoelectrowetting (SCOEW) device [15,16] that requires no cover plate and therefore allows unimpeded access to the droplets on the chip.

Although SCOEW devices are structurally simple, the droplet driving mechanism is relatively complex, and it is relatively easy to drive droplets only in the direction of the transverse electric field. Without two-dimensional manipulation, SCOEW devices are unable to realize some essential functions, such as positioning the droplet in two dimensions, and coalescing two droplets that are not in line or bypassing another droplet in order to avoid coalescence. Even droplet mixing is considerably less efficient if the droplet is limited to a one-dimensional path [22,23]. Chiou et al. [24] in 2009 proposed a method using paired diamond (PD)-shaped light patterns to form a potential gradient perpendicular to the direction of the electrodes. However, the magnitude of the driving force generated can only reach less than 40% of that in the x-direction.

Srinivas Akella et al. [25] in 2013 designed a chip with electrode pads in different directions to drive droplets in multiple directions by activating the electrode pairs in a certain direction. But such method

* Corresponding authors.
E-mail addresses: antoine_riaud@fudan.edu.cn (A. Riaud), jia.zhou@fudan.edu.cn (J. Zhou).

https://doi.org/10.1016/j.snb.2022.132231
Received 23 March 2022; Received in revised form 6 June 2022; Accepted 14 June 2022
Available online 16 June 2022

increases the number of electrodes and thus the complexity of the control signal.

In this paper, we propose a method to achieve two-dimensional manipulation of droplets using Z-shaped light patterns without adding electrodes. After introducing the underlying principles for the manipulation along arbitrary directions, we use a combination of experiments, analytical model and numerical simulations to explore the effect of the orientation of the pattern on the droplet motion, and optimize the pattern to efficiently move droplets in the y-direction. By unlocking the motion in the y-direction, this new light pattern brings the SCOEW technology closer to realizing its true potential.

2. Device structure and multi-directional drive principle

SCOEW chips are essentially two electrodes of opposite polarities separated by a photoconductive surface such as amorphous silicon (α-Si). For instance, the structure of the single-side continuous opto-electrowetting device used in this study is shown in Fig. 1(a). It is a 500 nm thick α-Si patterned onto a 25 × 25 mm^2 glass substrate. Two gold electrodes (thickness 100 nm with 5 nm chromium as the adhesion layer) are deposited by physical vapor deposition and patterned by photolithography on each side of the chip. This semiconductor is coated by a pair of dielectric and hydrophobic layers composed of 500 nm-thick SU8 and 2 μm of Teflon, respectively.

The most common light pattern used for droplet manipulation is a white background with a straight dark line passing between the electrodes that divides the photoconductive surface in two regions, one connected to each electrode with an electric potential U_0 intermediate between the positive and negative electrodes. (Fig. 1(a)). The resistivity of the semiconductor layer is modulated by the light intensity, and the resistance of R_3 under the dark pattern is greater than that of R_2 in the light. In an idealized view, the photoconductivity switches from 0 to infinity between dark and bright regions. Therefore, R_3 behaves like an open circuit, and the electric current must propagate inside the droplet (as an electric polarization) instead of inside the photoconductor. Thus, the electric charge of C_1 and C_2 combined must be the same as the charge of C_3, indicating a higher charge density in C_3, and therefore a higher voltage on the right side than on the left side., which results in a smaller contact angle on the right side as expressed by the Lippman-Young theory in Eq. (1). [26]:

$$\cos\theta = \cos\theta_0 + \frac{CU^2}{2\gamma}, \text{ where } U \le U_0 \tag{1}$$

where C is the areal capacitance of the combined dielectric and photoconductor. If the dark line does not cross the droplet by the middle, the electrowetting voltage becomes larger in the smaller half of the droplet. This induces a stronger electrowetting effect that acts as restoring force to pull back the droplet to the middle of the black line. Therefore, the droplet is securely trapped on the black line.

In our experiments, the chip was installed on an optical platform combining a video projector (BENQ-MU006) and 200 mm focal lens (Thorlabs-LA1417-A/N-BK7) to project the video projector image onto the chip. Light patterns for droplet driving were generated with Python. For the accuracy of the drive, we first aligned the coordinate of the projection image and the chip, defining the direction between two electrodes as x. The droplets were introduced with a pipette. To reduce evaporation, droplet tests were carried out in silicone oil (Sinopharm Chemical Reagent) with the viscosity of 1.5 cSt.

Similar to previous works, a dark stripe (named as the *driving segment*) passes through the droplet with a direction perpendicular to the intended motion of the drop. However, the dark stripe alone does not allow multidimensional driving because it does not separate the electrodes from one to another and would trigger a short-circuit instead of moving the droplet. To prevent those short-circuits, we introduce a more complex light pattern where the driving segment is complemented by two notches that ensure the suitable division of the chip (Fig. 1b). The current flowing from the positive terminal is blocked by the notch and flows through the illuminated part, i.e., from one side of the driving segment to the other, thus forming a potential gradient in the direction perpendicular to the driving segment, i.e., the potential gradient in the y-direction. Through this way we achieved the y-directional movement of the droplet (See SI video1).

Successive video screenshots of the droplet drive are shown in Fig. 1 (c-f). A yellow droplet was driven along the x-direction from 3.10 s to 8.59 s, then the pattern was switched to Z-shaped pattern, and the

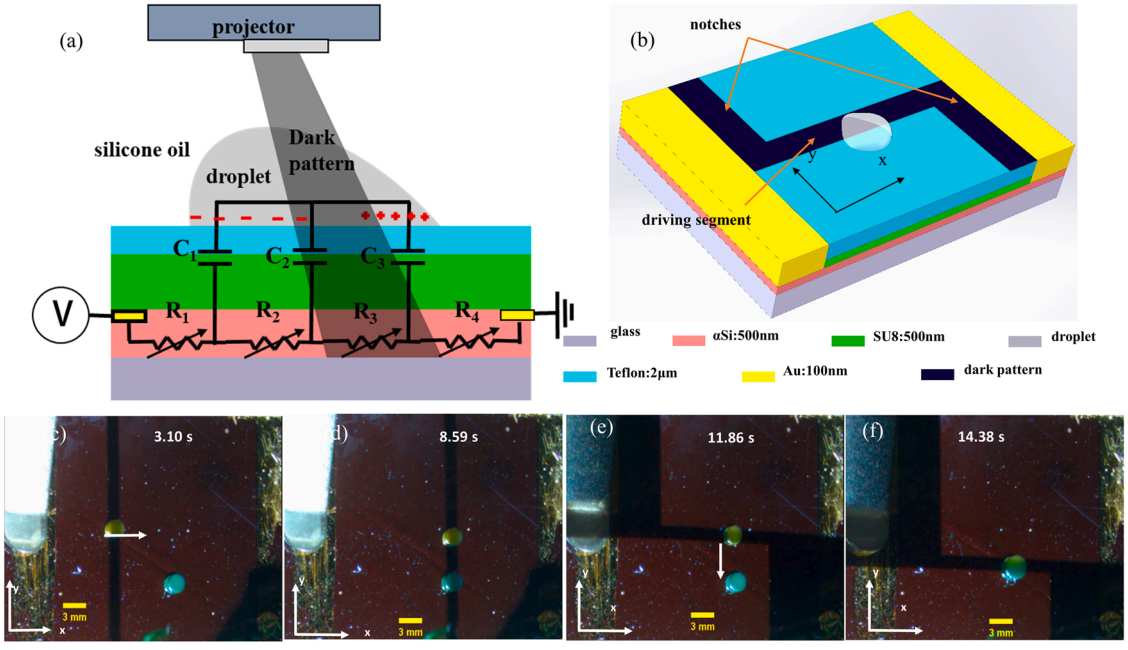

Fig. 1. Schematics of (a) SCOEW chip schematic and its equivalent circuit model. (b) SCOEW chip structure with the Z-shaped light pattern for droplet driving in the y direction; (c-d). a yellow droplet is moved in the x-direction from 3.10 to 8.59 s; (e-f) the yellow droplet is moved in the y-direction from 11.86 to 14.38 s and is merged with a blue droplet.

yellow droplet was driven along the y-direction until it coalesced with the blue droplet from 11.86s to 14.38 s. More generally, adjusting the direction of the driving segment allows driving the droplet along arbitrary directions (30°, 45° and 60° drives are shown in SI video 2,3,4 respectively). Next, we provide an overview of the key parameters for the design of the Z-shaped patterns and derive a simplified model to estimate the likelihood of droplet motion.

3. Results

3.1. Drive capability in different directions

When a droplet is exposed to external forces (such as gravity or electrocapillarity), its contact line remains pinned unless the force exceeds some unpinning threshold that depends on the contact angle hysteresis. Therefore, a primary concern is to evaluate this minimum voltage needed to trigger a droplet motion in different directions using the Z-shaped light pattern. Fig. 2(a) shows the minimum driving voltage for DI water with volumes ranging from 0.5 μL to 10 μL. The driving segment width is 0.5–1 times the droplet diameter. Regardless of the droplet volume, droplet motion is almost always harder to achieve in the y-direction than in the 45° direction, which itself is harder than in the x-direction.

In order to move, the droplet contact line must unpin: the contact angle at the droplet front must exceed the advancing contact angle, and the contact angle at the droplet back must drop below the receding contact angle [27,28]. Experimental contact angles θ for different actuation directions and actuation voltages are shown in Fig. 2(b). The contact angle change $\Delta\theta$ in the y-direction (4°) is nearly 8 times smaller than in the x-direction (30°). Therefore, in order to achieve a similar driving force and overcome hysteresis effects, the bias voltage must be increased when driving droplets in the y-direction. For instance, doubling the voltage from 100 V to 200 V yields a bigger change in contact angle in the 45° direction than when using 100 V in the x-direction (Fig. 2(b)). This means that larger voltages are needed in the oblique direction to trigger droplet motion than along the direction of the electric field.

In order to identify the cause for this reduced driving ability, the SCOEW was simulated in three dimensions with a finite-element model (more details see SI1): the substrate is modeled as a stack of a two-dimensional ohmic plate (the photoconductive layer) and a two-dimensional dielectric (the dielectric layer). The droplet is a three-dimensional ohmic body that can be polarized by the dielectric layer. In the model, the light pattern sets the conductivity of the photoconductive layer, and the voltage between this layer and the droplet surface gives the contact angle according to Eq.(1). An asymmetric voltage drop indicates an asymmetric contact angle and therefore a nonvanishing electrowetting force acting on the droplet.

The simulated contact angle varies along the perimeter of the droplet (Fig. 2(c)), with the greatest change relatively close to the direction of motion, *i.e.* $\pi/4$ and $\pi/2$ for the 45° and y-directions, respectively. The contact angle change for y direction (7.03°) is almost 4.3 times weaker than in the x-direction (29.12°), with the 45° case taking an intermediate value (17.13°), which is consistent with the experimental trend.

Since the variation of the contact angle is due to the voltage difference U across the dielectric, we compute this voltage for the x, 45° and y-directions (Fig. 2(d-f),respectively). In all cases, $|U|$ is larger at the front of the droplet than at the back, which indicates a forward electrowetting driving force until the droplet reaches the middle of the dark line. Regarding the loss of driving force, we note that the front-back dielectric voltage difference $U^2_{front} - U^2_{back}$ is larger in the x-direction (1175 V^2) than in the 45° angle or y-direction (628 V^2 and 231 V^2, respectively). For a given bias voltage U_0. This results in a reduced difference in contact angle, which makes it more difficult to unpin the droplet and trigger motion along an oblique direction.

In order to address this reduced driving ability, we next optimize the

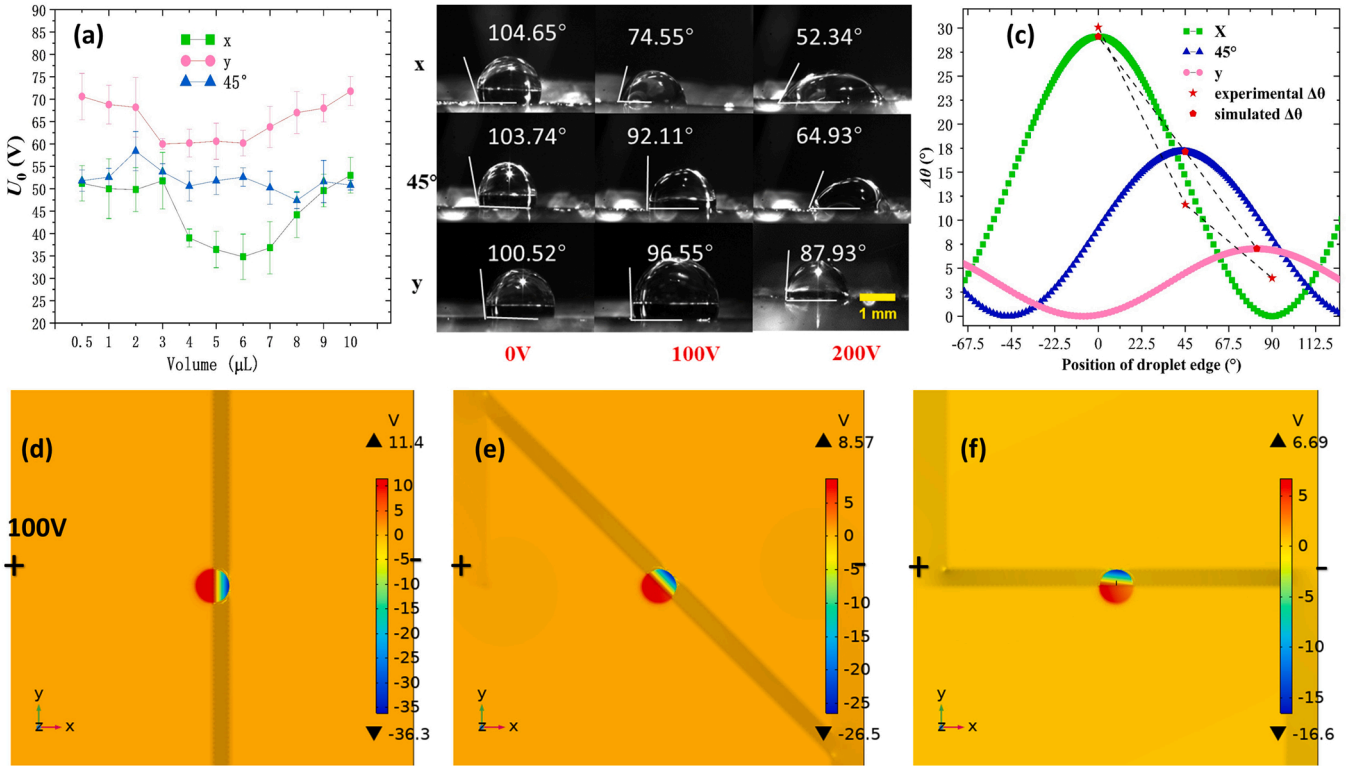

Fig. 2. (a) Experimental minimum driving voltage in x/45°/y–direction for different droplet volumes. (b). Experimental droplet contact angle in x/45°/y-direction for increasing voltage; (c). Simulation of contact angle variation along the contact line with x/45°/y-direction driving segments; (d-f) simulated voltage drop across the dielectric in the x/45°/y-direction, respectively.

light pattern to achieve droplet motion in the y-direction.

3.2. Optimization of the drive capability in the y-direction

According to Fig. 2(d-f), the reduced driving ability is due to a decreased voltage drop U across the dielectric. Hence, in order to improve the driving ability of the SCOEW in the y-direction, we first derive a simplified model to compute U. The aim is to refine the inequality $U \leq U_0$ in Eq. (1). In our simplified model, we designate by V_2 and V_3 the electric potential in the photoconductive layer under the front and the back of the droplet, respectively. Then the droplet potential V satisfies $V_2 \leq V \leq V_3$. Subtracting V_2, we find that the voltage U between the droplet and the dielectric layer (used in Eq. 1) satisfies: $0 \leq U \leq U_{d3}$, with $U_{d3} = V_3 - V_2$.

We estimate U_{d3} using the equivalent circuit model shown in Fig. 3 (a). When U_0 is applied, the resistances R_{d1} and R_{d2} of the notches are larger than the resistances R_{l1} and R_{l2} in the illuminated part, resulting in a greater current to flow through the illuminated parts which is shown in orange arrows in Fig. 3(a). Therefore, in the y direction, there is a voltage increase of U_{d3} over the resistance R_{d3}, which is given by Eq. (2):

$$U_{d3} = \frac{U_0(R_{d1} - R_{l2})}{R_{d1} + R_{l1} + 2R_{d1}R_{l1}/R_{d3}}, \tag{2}$$

where we assumed $R_{d1} = R_{d2}$ and $R_{l1} = R_{l2}$ (See SI2). Such a voltage drop reduces the droplet contact angle (See Eq. (1)) and the droplet can be moved along with the driving segment. We also note that light pattern of previous studies, lacking notches, would feature $R_{d1} = R_{l1}$ and $R_{d2} = R_{l2}$, which would yield a zero-voltage therefore be unsuitable to drive the droplet.

To improve the driving ability of the droplet along the y-direction, *i.e.* to increase U_{d3}, we identify two independent parameters: the width of the notches (w) and the width of the driving segment (L_3). Assuming that the current flows exclusively in the x-direction, except for the driving segment where it flows exclusively in the y-direction, and assuming that the electric potential only varies in the direction of the electric current, we substitute simple one-dimensional resistance expressions into Eq. (2) (See SI3 for the detailed calculation):

$$U_{d3} = \frac{U_0(w\rho_d + w\rho_l - L_1\rho_l)}{w\rho_d - w\rho_l + L_1\rho_l + \rho_l 4w(L_1 - w)(L_1 - 2w)/L_1L_3}. \tag{3}$$

According to Eq. (3), increasing the driving segment width L_3 increases the maximum voltage drop and therefore the driving segment should be as wide as possible (that is, approximately the droplet diameter). From Eq. (2), we infer that increasing the width w of the notches will increase R_{d1} and R_{d2}, and decrease R_{l1} and R_{l2}, which will increase U_{d3}. This is confirmed numerically in Fig. 3(b) with $L_3 = 3$ mm, the light conductivity $\rho_l = 1.789 \times 10^5$ and the dark conductivity $\rho_d = 3.943 \times 10^6$ Ω⊡cm respectively (see SI4) under the bias voltage of 100 V. To a large extent, theoretical data agrees quantitatively well with experiments using 4 μL DI water droplets (Fig. 3(b)). Moreover, the minimum contact angle for each w that we obtained using Comsol simulation also corresponds to the theoretical model and experimental values, although the values in the simulation results are slightly less than the theoretical and experimental values.

Simulations and experimental data show that increasing the notch width allows decreasing the contact angle from 105° to 72.6°, which is similar to what can be obtained when driving droplets in the x-direction (Fig. 2(b)); the inserted figure in Fig. 3(b) shows the voltage reduction in the simulation results. At larger w, some droplets unpin and begin to move, so experimental results include the advancing (A) and receding contact angles (R) for unpinned droplets. We tested the variation of contact angle with U^2 for different w, (SI Fig. S4). As w increases, the range of the contact angle variation increases which is consistent with simulation results. However, the inflected shape of the $cos\theta - U^2$curves is markedly different from the Lippman-Young modelshown in Fig. 3(c), which has a parabolic shape unlike the straight line expected from Eq. (1). This may be due to the saturation of the electrowetting effect, but also to variations of the capacitance of the combined photoconductive/dielectric layers. The latter is due to carrier depletion in the

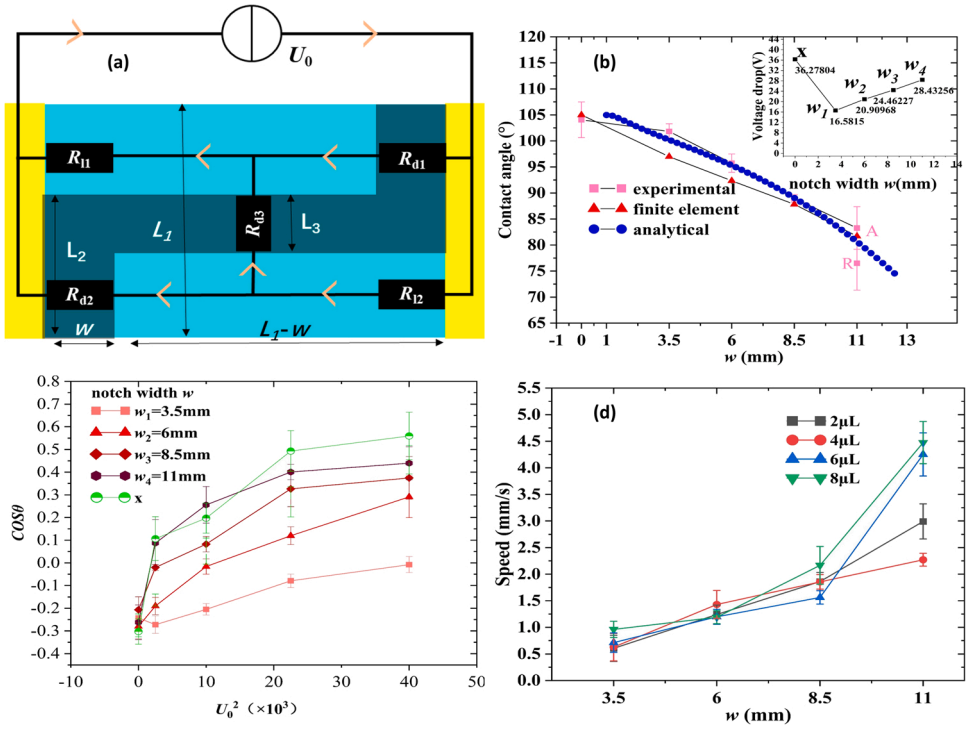

Fig. 3. Optimization of SCOEW chip with Z-shaped pattern (a) equivalent circuit schematic, current direction is marked with orange arrows. (b) experimental, simulated and analytical contact angle variation depending on the driving segment width (w) at $U_0 = 100$ V.(c) experimental contact angle depending on the bias voltage U_0^2(five tests for each point). (d) droplet moving speed depending on the driving segment width w.

photoconducting layer, which is common in metal-oxide semiconductor capacitor (MOSCAP). By increasing *w*, the ability of driving in the y-direction (characterized here by the change in contact angle) has reached the level of the x-direction (green line in Fig. 3(c)). Fig. 3(d) shows that the drive speed increases as *w* increases, with a maximum drive speed of 4.86 mm/s for a 8 μL stained DI water (see SI video5).

4. Conclusion

Droplet digital microfluidics based on electrowetting have long faced a wiring bottleneck. The single-sided continuous optoelectrowetting (SCOEW) promises to address this issue by using dynamic light pattern to control droplet motion, but has so far been limited to the difficulty of manipulating droplets in two-dimensions. Here, we have introduced and optimized a Z-shaped light pattern that can drive droplets in arbitrary directions. The driving mechanism is well explained by a finite element model and an analytical model. Our careful analysis also highlights some key differences between EWOD and SCOEW physics, such as an apparent failure of the Young-Lippmann law. The multidimensional droplet driving demonstrated in this work already enables merging droplets that are not in line, and is also an important prerequisite to achieve efficient droplet mixing, and bypassing droplets to avoid coalescence.

CRediT authorship contribution statement

Enqing Liu: Experimental design, experimental implementation, finite element simulation, data organization, first draft of manuscript writing, manuscript revision. **Cui Wang**: Software design, experimental data proofreading, manuscript revision. **Hanyun Zheng**: Software design, experimental data proofreading. **Shuren Song**: Figures editing. **Antoine Riaud**: Experimental ideas guidance, theoretical analysis guidance, finite element simulation, manuscript revision. **Jia Zhou**: Project proposal design, experiment idea guidance, manuscript writing guidance, manuscript revision.

Declaration of Competing Interest

The authors declare the following financial interests/personal relationships which may be considered as potential competing interests: Jia Zhou reports financial support was provided by National Natural Science Foundation of China with Grant Nos. 61874033. Jia Zhou has patent #202111627615.3 issued to Jia Zhou.

Acknowledgement

This work was supported by the National Natural Science Foundation of China with Grant Nos. 61874033 and 12004078, 51950410582, the State Key Lab of ASIC and System State Key, Fudan University with Grant Nos. 2021MS001 and 2021MS002, and Science and Technology Commission of Shanghai Municipality with Grant Nos. 22QA1400900 and 22WZ2502200.

Appendix A. Supporting information

Supplementary data associated with this article can be found in the online version at doi:10.1016/j.snb.2022.132231.

References

[1] L.M. Wilder, J.R. Thompson, R.M. Crooks, Electrochemical pH regulation in droplet microfluidics, Lab Chip 22 (3) (2022) 632–640, https://doi.org/10.1039/d1lc00952d.
[2] Y. Yu, J. Chen, S. Yang, S.-K. Fan, J. Zhou, A monolithic lab-on-a-chip for electrochemical detection presented at the 2012 IEEE 11TH International Conference on Solid-state and Integrated Circuit Technology (ICSICT-2012), Xian, China, pp. 157–159.
[3] A.L. Culberson, M.A. Chilmonczyk, P.A. Kottke, A.C. Bowles-Welch, D. Ghoshal, A. G. Fedorov, Sample-to-analysis platform for rapid intracellular mass spectrometry from small numbers of cells, Lab Chip 21 (23) (2021) 4696–4706, https://doi.org/10.1039/d1lc00884f.
[4] G. Shabestani Monfared, P. Ertl, M. Rothbauer, Microfluidic and lab-on-a-chip systems for cutaneous wound healing studies pharmaceutics 13 (6) (2021) 10.3390/pharmaceutics13060793.
[5] X. Zeng, K. Zhang, J. Pan, G. Chen, A.Q. Liu, S.K. Fan, J. Zhou, Chemiluminescence detector based on a single planar transparent digital microfluidic device, Lab Chip 13 (14) (2013) 2714–2720, https://doi.org/10.1039/c3lc50170a.
[6] Yuhua Yu, Jianfeng Chen, Jia Zhou, Parallel-plate lab-on-a-chip based on digital microfluidics for on-chip electrochemical analysis, J. Micromech. Microeng. 24 (1) (2014), https://doi.org/10.1088/0960-1317/24/1/015020.
[7] J. Lee, H. Moon, J. Fowler, C.-J. Kim, T. Schoellhammer, Addressable micro liquid handling by electric control of surface tension presented at the 14th IEEE International Conference on Micro Electro Mechanical Systems (MEMS 2001), Interlaken, Switzerland, 2001, pp. 499–502.
[8] J. Li, C.C. Kim, Current commercialization status of electrowetting-on-dielectric (EWOD) digital microfluidics, Lab Chip 20 (10) (2020) 1705–1712, https://doi.org/10.1039/d0lc00144a.
[9] X. Rui, S. Song, W. Wang, J. Zhou, Applications of electrowetting-on-dielectric (EWOD) technology for droplet digital PCR, Biomicrofluidics 14 (6) (2020), 061503, https://doi.org/10.1063/5.0021177.
[10] Tai-Hsuan Lin, Da-Jeng Yao, Applications of EWOD systems for DNA reaction and analysis, J. Adhes. Sci. Technol. 26 (12–17) (2012) 1789–1804, https://doi.org/10.1163/156856111×600578.
[11] Liang Zhu, Yanying Feng, Xiongying Ye, Jinyang Feng, Yanbin Wu, Zhaoying Zhou, An ELISA chip based on an EWOD microfluidic platform, J. Adhes. Sci. Technol. 26 (12–17) (2012) 2113–2124, https://doi.org/10.1163/156856111×600172.
[12] M.N. Tsaloglou, A. Jacobs, H. Morgan, A fluorogenic heterogeneous immunoassay for cardiac muscle troponin cTnI on a digital microfluidic device, Anal. Bioanal. Chem. 406 (24) (2014) 5967–5976, https://doi.org/10.1007/s00216-014-7997-z.
[13] Wei Wang, Xichuan Rui, Wenjie Sheng, Qing Wang, Qi Wang, Kaidi Zhang, Antoine Riaud, Jia Zhou, An asymmetric electrode for directional droplet motion on digital microfluidic platforms, Sens. Actuators B Chem. 324 (2020), https://doi.org/10.1016/j.snb.2020.128763.
[14] H. Wu, R. Dey, I. Siretanu, D. van den Ende, L. Shui, G. Zhou, F. Mugele, Electrically controlled localized charge trapping at amorphous fluoropolymer-electrolyte interfaces, Small 16 (2) (2020), e1905726, https://doi.org/10.1002/smll.201905726.
[15] S.Y. Park, M.A. Teitell, E.P. Chiou, Single-sided continuous optoelectrowetting (SCOEW) for droplet manipulation with light patterns, Lab Chip 10 (13) (2010) 1655–1661, https://doi.org/10.1039/c001324b.
[16] D. Jiang, S.Y. Park, Light-driven 3D droplet manipulation on flexible optoelectrowetting devices fabricated by a simple spin-coating method, Lab Chip 16 (10) (2016) 1831–1839, https://doi.org/10.1039/c6lc00293e.
[17] J.K. Valley, S.N. Pei, S.L. Neale, A. Jamshidi, H.-Y. Hsu, M.C. Wu, Light-actuated digital microfluidics for large-scale parallel manipulation of arbitrarily sized droplets presented at the 23rd IEEE International Conference on Micro Electro Mechanical Systems (MEMS 2010), Hong Kong, China, 2010, pp. 252–255.
[18] Pei Yu Chiou, Hyejin Moon, Hiroshi Toshiyoshi, Chang-Jin Kim, Ming C. Wu, Light actuation of liquid by optoelectrowetting, Sens. Actuators A Phys. 104 (3) (2003) 222–228, https://doi.org/10.1016/s0924-4247(03)00024-4.
[19] J.K. Valley, S.N. Pei, A. Jamshidi, H.Y. Hsu, M.C. Wu, A unified platform for optoelectrowetting and optoelectronic tweezers, Lab Chip 11 (7) (2011) 1292–1297, https://doi.org/10.1039/c0lc00568a.
[20] S. Park, C. Pan, T.H. Wu, C. Kloss, S. Kalim, C.E. Callahan, M. Teitell, E.P. Chiou, Continuous optoelectrowetting for picoliter droplet manipulation, Appl. Phys. Lett. 92 (15) (2008) 151101–1511013, https://doi.org/10.1063/1.2906362.
[21] P.Y. Chiou, A.T. Ohta, M.C. Wu, Massively parallel manipulation of single cells and microparticles using optical images, Nature 436 (7049) (2005) 370–372, https://doi.org/10.1038/nature03831.
[22] H.W. Lu, F. Bottausci, J.D. Fowler, A.L. Bertozzi, C. Meinhart, C.J. Kim, A study of EWOD-driven droplets by PIV investigation, Lab Chip 8 (3) (2008) 456–461, https://doi.org/10.1039/b717141b.
[23] J. Fowler, M. Hyejin, K. Chang-Jin, Technical Digest. MEMS 2002 IEEE International Conference. Fifteenth IEEE International Conference on Micro Electro Mechanical Systems (Cat. No.02CH37266), 2002, pp. 97–100.
[24] S.Y. Park, S. Kalim, C. Callahan, M.A. Teitell, E.P. Chiou, A light-induced dielectrophoretic droplet manipulation platform, Lab Chip 9 (22) (2009) 3228–3235, https://doi.org/10.1039/b909158k.
[25] V. Shekar, M. Campbell, S. Akella, Towards automated optoelectrowetting on dielectric devices for multi-axis droplet manipulation presented at the IEEE International Conference on Robotics and Automation (ICRA), Karlsruhe, Germany, 2013.
[26] Frieder Mugele, Jean-Christophe Baret, Electrowetting: from basics to applications, J. Phys. Condens. Matter 17 (28) (2005) R705–R774, https://doi.org/10.1088/0953-8984/17/28/r01.
[27] Wei Wang, Qi Wang, Kaidi Zhang, Xubo Wang, Antoine Riaud, Jia Zhou, On-demand contact line pinning during droplet evaporation, Sens. Actuators B Chem. 312 (2020), https://doi.org/10.1016/j.snb.2020.127983.
[28] Wei Wang, Qi Wang, Jia Zhou, Antoine Riaud, Observation of contact angle hysteresis due to inhomogeneous electric fields, Commun. Phys. 4 (1) (2021), https://doi.org/10.1038/s42005-021-00691-4.

Enqing Liu is currently pursuing a doctoral degree in the State Key Laboratory of ASIC and System, School of Microelectronics, Fudan University. His research interest focuses on lab-on-a-chip , digital microfluidic technology and intelligent photo-controlled microfluidic system.

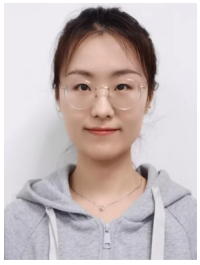

Cui Wang is currently pursuing the master degree with the State Key Laboratory of ASIC and Systems, School of Microelectronics, Fudan University. Her research interest focuses on AI-powered digital microfluidics based on opto-electrowetting.

Shuren Song is currently pursuing a doctoral degree in the State Key Laboratory of ASIC and System, School of Microelectronics, Fudan University. His research interest focuses on acoustic streaming in microdroplets and multiphase microflow modeling.

Hanyun Zheng is currently pursuing the degree with the State Key Laboratory of ASIC and Systems, School of Microelectronics, Fudan University. Her research interest focuses on OEW devices automatic control and its applications in biology.

Antoine Riaud received his Ph.D. degree in acoustics, microelectronics and telecommunications from Lille University (France) in 2017, and then did a postdoc at Paris Descartes University. Since 2018, he has joined Fudan University (Shanghai, China) as associate professor. His research interests are microfluidics, acoustofluidics, electrowetting, and other technologies for microbiosamples processing. He has authored/co-authored over 37 peer-reviewed journal publications in these fields and has 6 issued or pending EU/international patents.

Jia Zhou received the Ph.D. degree from Fudan University in 2004. She is currently a Professor in the State Key Laboratory of ASIC and System, School of Microelectronics, Fudan University. Her research interests are in nano/microfluidics, MEMS/NEMS-based chemical, biochemical and biomedical sensors.